[1] **Abdullah J. H. Al Gizi1**

[2] **Wadullah Jaleel Mhawes Hatem**

Realization of a Novel Artificial Intelligence Fuzzy Controller with Solar Irradiance-altered Maximum Power

Journal of Electrical Systems

Abstract: **-** This paper reports the realization of a novel artificial intelligence fuzzy Logic controller (AI-FLC) that attained the optimum power of the photovoltaic cell (PV array) with solar irradiance altered (from 300 to 1000 w/m2) using the boost-converter circuit. Experiments were conducted using the Simulink /MATLAB coding. The nonlinear current-voltage character of the PV array was observed to be affected by the weather conditions, solar irradiance level, and ambient temperature. In addition, unique maximum power point for each irradiance level was achieved which was ascribed to the rapid response of the FLC to the atmospheric changes without requiring any system parameters. The obtained accuracy was as much as 98.875%. The post converter circuit was connected to the buck converter for taking the advantage of the generated power, thereby stabilizing the synchronous generator-emanated voltage. The response of the proposed system was demonstrated to be better than the conventional PD control, wherein the output voltage was stable at 220 V even at low levels of the solar irradiance.

Keywords: Solar Irradiance, Boost-Converter, Buck-Converter, PD Control .

I. INTRODUCTION

The body text without an indent is shown here. the text within the body as a preventative step against environmental pollution and climate change, research into renewable energies has increased in recent years. We must find affordable, abundant, clean energy sources, such as solar energy, as fossil fuel alternatives for sustainable development due to the world's growing population, pollution, and seeming increase in the use of fossil fuels. However, additional issues still prevent the technology from being extensively employed, such as the high initial cost and poor competency (only 20%) of solar energy. In order to do this, we investigate the best option in an effort to overcome the challenges. [1]quantity of power produced as a result of changing meteorological conditions, solar radiation, and ambient temperatures. Typically, solar-powered devices consist of photovoltaic (PV) collections of various a combination of sizes and shapes a variety of customs to generate a straight current (DC) that is then converted into an alternating current (AC) by means of DC / AC inverters.[2] [3, 4] By reaching the peak of the I-V characteristics, known as the all-out each in PowerPoint (MPP) worth in terms of solar irradiation and fever, these inverters are employed to achieve the optimal power of the PV arrays. A solar cell's typical value is specified at 1000 W/m2 of solar radiation and a 25 degrees Celsius[5] [6, 7]. The inverters that are connected to the output of the PV cells to control the duty cycle requirements of the incoming pulse-width modulations (PWM), which feed the gate of the MOSFET, IGBT, or any other semiconductor electric change to intensify or minimize the PV cell voltages to spread the MPP. Numerous appropriate methods, including incremental conductance MPPT, are used for this drive.[8], trouble and detect (P & O) [9]fuzzy logic switch (FLC) [10]so forth. The FLC technique is advantageous because it differs from standard controllers' procedures and is similar to the proportional-integral-derivative supervisor (PID) procedure in that it does not require any knowledge of the scheme limits. The limitations of the PV array, convertors, generators, or any other scheme are not necessary in order to obtain these values because the fuzzy logic managers only require two inputs and one output in situations where the efforts result in errors and modifications of errors (for example, the PV arrays power and voltage modification standards). The FL managers are distinguished by their solid recital, stronghold, heftiness, and continued sincerity regardless of the linear or nonlinear terrain of the plan, and they do not need to write the transfer component of the scheme.

Figure 1 represents the graphical presentation of a simple PV collection power generation scheme without any connection to the national grid (direct-coupled scheme) and series energy storing.[11]. Here, the voltage is first increased using a boost messenger to reach the maximum-power-point, and then it is decreased using a simple

[1]*Corresponding author: Thi-Qar Technical Collage, Southern Technical University, Iraq

[2]Basrh Technical Collage, Southern Technical University, Iraq

converter while simultaneously controlling the innervation field coil voltage of a single-phase synchronic generator to regulate the output voltage of the generator. The FLC has two skilled convertors.

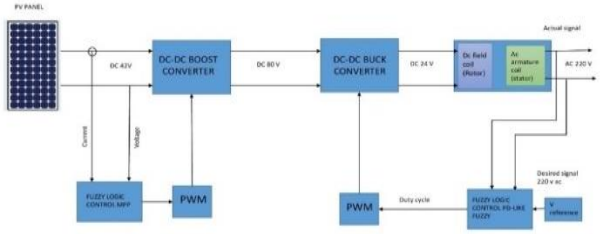

Figure 1. Schematic presentation of a typical PV system MPPT algorithm and PD-like fuzzy control

Numerous messenger subtypes have been industrialized over time. For instance, Kim and colleagues [12] employed the menial messenger to keep a phone Using the FLC, cordless completed a PV system in a tiny grid using MPPT. They examined the results as well as the method for creating the rule-base and association purposes in great detail. When the energy from the solar panel changed into finished electric lighting, the FLC's ability to reach full power was established. Shain and co. [13-15]Plan six distinct methods for utilizing various fuzzy contributions with the increase convertor to maximize the power of the PV cells. It used a purpose chart for the association and a rule-base table for each case to compare various approaches' compensations and challenges. It was revealed that FLC-based regulator schemes use deceptive methods to create the rule-base and select the particular kinds of association purposes. To upsurge correctness, Liu et al [16, 17] accessible process for creating a purpose for an association for an external to zero input signal. This strategy was contrasted with the established method that accounts for the regular varieties to total the close effects. Whereas the goal of our study is to stabilize the solar cells' unpredictable voltages, powers, and currents so that we can provide the load difference. In addition, the duty cycle that effectively controlled the PWM or the load was adjusted, causing the convertor voltage to vary.

As a result of our research, Through an AVR back-feeding fuzzy control circuit that functions like PD, the generator's excitation field voltage was managed. In order to compare the feedback with the reference voltage and mistakes, the 220 V generator output was used. 96.7 to 99.8% of the MPP algorithm's first stage was correctly predicted by the system. Additionally, the excitation field's voltage and current showed extremely high levels of stability. The combined MPP and AVR system demonstrated great stability even at low solar irradiation (300 W/m2). Although the sun irradiation abruptly changed, the output voltage remained constant.

II. EQUIVALENT CIRCUIT (E.CCT) OF A SOLAR CELL WITH COMPONENTS

To know the process of a astral cell, it is usual to present its equal circuit in footings of ass electric devices (Figure 2). The solar cell contained of a present basis linked in parallel to a diode and confrontations (together parallel and sequence), however it cannot be attained but in repetition. A straight current (I_{ph}) is shaped in the PV array (made of silicon or germanium) when the solar radiation falls on the semiconductor, where the corresponding current (I_d) and voltage (V_d) of the diode. The parallel-resistance (R_p) is due to the superficial inhomogeneity and current loss at the limits of the solar cell which can be excessive. The series resistance (R_s) is originated from the confrontation of silicon and interaction confrontation of the physical which is very low (≈ 1 ohm). The V and I of the solar-cell is I_{pv} and V_{pv}, respectively.

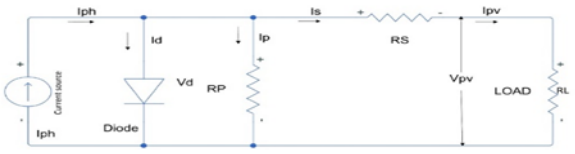

Figure 1. Corresponding circuit of a typical solar cell The existing voltage relations of the cell can be written as:

$$I_{pv} = I_{load} = I_S = I_{ph} - (I_d + I_p) \quad (1)$$

$$I_d = I_O \times [e^{q.\frac{(V_{pv}+I_{sR_S})}{nKT}} - 1] \quad (2)$$

$$I_{load} = I_{ph} - I_O \times \left[e^{q.\frac{(V_{pv}+I_{sR_S})}{nKT}} - 1\right] - \frac{V_{pv}+I_{sR_S}}{R_p} \quad (3)$$

where I_O(A) is the PV array opposite soaked existing (fullness existing of the crystal rectifier), I_{pv}(A) signifies the PV-current, Q (1.602 × 10^{-19} C) is the electronic- charge, n signifies the non-idealist aspect of the crystal rectifier connexion, K (1.38× 10^{-23} J/K) is the Boltzmann-constant, and T is the clement of the p-n Joint[18-20].Figure 2 displays a single-solar cell corresponding to the corresponding circuit in Figure 2 via the interaction with numerous solar cells both in parallel and series to constitute a "PV array". Low power in the range of a single solar cell of 1 to 1.5 watts. Thus, a large number of cells can be combining them in accordance with the desired worth of the currents, voltages, and powers.

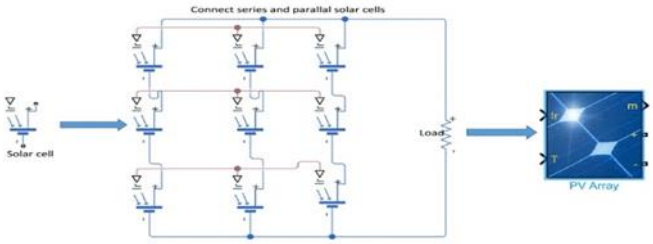

Figure 2. Architecture of a PV array composed of a group of solar cells

III. MAXIMUM POWER POINT (MPP)

In this education, a humble MATLAB imitation of a photovoltaic array covering mutable confrontation and continuous capacitor was achieved to comprehend the MPP (Figure 4). The unhurried flows, output voltages and power gotten at a secure infection and altering the sun's irradiances were likened with the one calculated at secure solar irradiance and numerous infections. A association was industrialised amongst the intended I &V presentation the stipulations within the PV collection.

Table 1. Stipulations of the future PV array

PV	Sanyo Electric of Panasonic Group VBHN 220 AA 01
$P_{max.}$	220.759 W
$V_{o.c}$	52.3 V
$I_{s.c}$	5.35 A
V_{max}	42.7 V
I_{max}	5.17 A

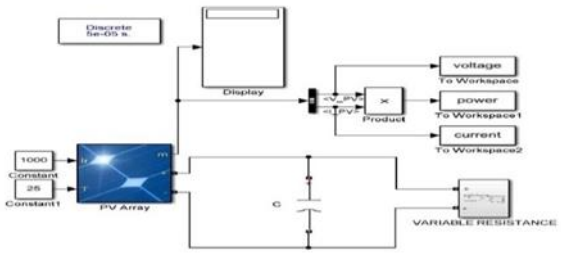

Figure 3. Circuit plan of the deliberate solar power system

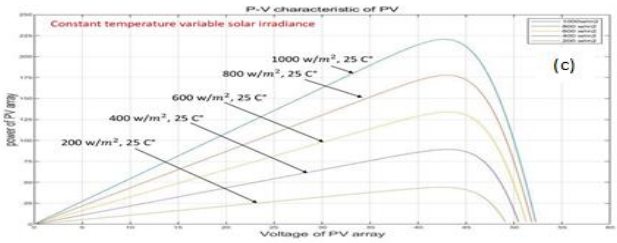

Figure **4** (a), (b), (c) and (d) exemplifies the P-V and I-V features of the PV-array at numerous infections and ordinances. The MMP was reached at a certain I and V, signifying a shift in the resilience of created scenarios to the I or V vicissitudes. The freight conflict altered as a result, pretentiously altering the quantity flowing through the PV-array. Temperature increases reduced PV power, although solar radiation increased it.

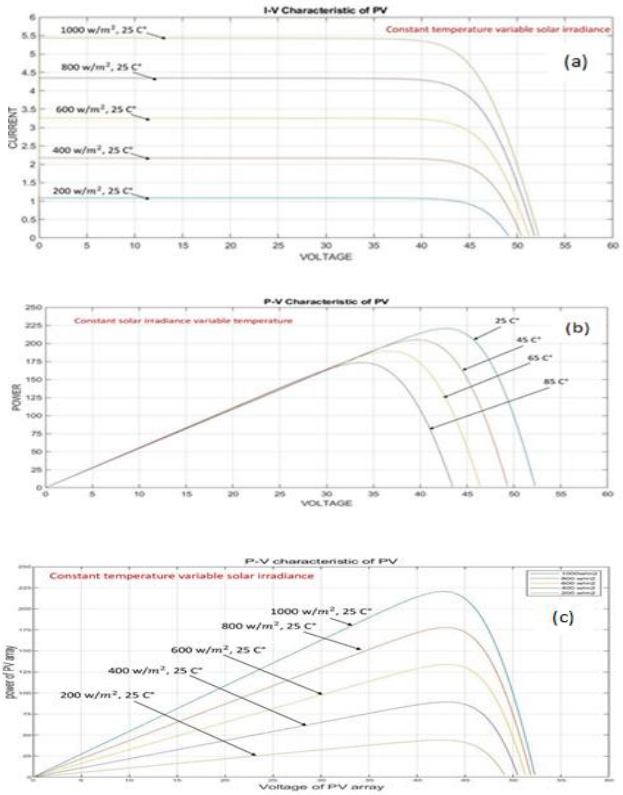

Figure 4. P-V features of the PV-array at frequent (a) irradiances and (b) temperatures; I-V features at dissimilar (c) temperatures and (d) irradiances

IV. RELATION BETWEEN MPP BEHAVIOUR AND FLC

Exhibitions the P-V features of the solar power system alienated interested in dual-parts. In the rightward part, the alteration in the influence is great for a minor difference of the voltage. Equally, in the left helping the alteration power and voltage are nearly the similar. In fact, the difference is minor in together cases whichever about or in the area actual nearby to the MPP. The FLC utilized 2 inputs and 1 output, where the P & V difference was rummage-sale at dual contributions or the error & mistake vicissitudes were used. Frequent kinds of contributions were used to control the current alteration with the power change.

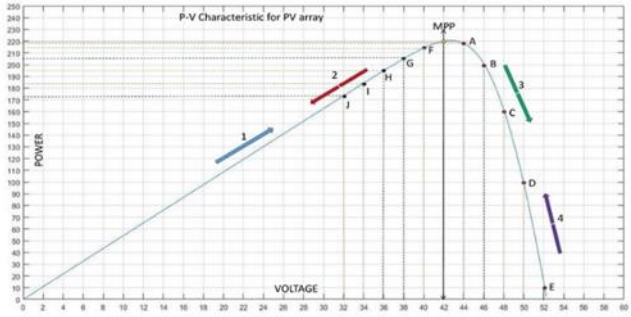

Figure 5. Power-voltage characteristics of the PV array

Next terms were usage to compute the modification of the V, P, error, and mistake difference.

$$\Delta P = P(t) - P(t-1) \quad (4)$$

$$\Delta V = V(t) - V(t-1) \quad (5)$$

$$E(t) = \frac{\Delta P}{\Delta V} = \frac{P(t)-P(t-1)}{V(t)-V(t-1)} \quad (6)$$

$$CE(t) = E(t) - E(t-1) \quad (7)$$

The position ΔP is the output regulation and the outputs of plants t and (t-1) are P(t) and P(t-1). ΔV the voltages at times t and (t-1) are denoted by the notations V(t) and V(t-1). The errors at times t and (t-1) are denoted by E(t) and E(t-1),CE(t) does not fit.

The reckonings obviously show which the power alteration is undesirable at (arrow3) away from the MPP, and the voltage (together are on the right side) is positive (missile 4). Though, the difference of together P & V are undesirable (arrow2) or optimistic (arrow1) As the credibility on the left side of the MPP adjustment, E(t) is always averse to the correct of the MPP and optimistic to the left of it. The next Table 2 values obtained against the checked PV array are advertised where the voltage adjustment is safe at 2 V and the power has been changed to be reflected elsewhere in the point.

The consequences in Table 2 obviously designated the heftiness of the by means of the Fuzzy rules for location up the whole trial. Within the display ponder, the double commitments of FLC formed perceived fresh measures (modification in control and voltage) whereby the fuzzification for these values was carried out by changing them into the dialect values. For occasion, when the control was negative or positive with exceptionally incredible esteem it was implied as Negative Enormous (NB) or Positive Huge (PB), correspondingly. It took a novel esteem in the midst of zero and one in which its major esteem meant the exact one.

At that point, the novel values were worked into the fluffy suggestion motor (FIE) wrapped up a predetermined table and contrasted with one another. Finally, the differentiate was made wrapped up the Mamdani strategy. For instance, if P and V are both NB, the duty structure is PB. The voltage change was assigned to be negative and mind-blowing for negative and wonderful control modifications, causing the point to be emptied out of the MPP and resulting in bolt 2. In order to swiftly restore the point to the MPP after it had become absent during included, it was necessary to increase the voltage by PB. The remainder of Informational was constructed in a manner that was identical to that of Figure 6. A set of values were obtained for which there had been a complete defuzzification after all the data had been agreed upon in this manner. It reverted its conversion to the new standards. Figure 7 shows the aiming fluffy rationale framework[21, 22].

Table 2. The examined PV array's actual values for V, P, P, V, E, and CE

No.	Point	Row no.	P(t)-P(t-1)	V(t)-V(t-1)	ΔP	ΔV	E	CE
1	MPP to A	3	219-220	44-42	-1	2	-0.5	
2	A to B	3	200-2019	46-44	-19	2	-9.5	TRUE
3	B to C	3	160-200	48-46	-40	2	-20	TRUE

4	**C to D**	**3**	**100-160**	**50-48**	**-60**	**2**	**-30**	**TRUE**
5	**D to E**	**3**	**10-100**	**52-50**	**-90**	**2**	**-45**	**TRUE**
6	**E to D**	**4**	**100-10**	**50-52**	**90**	**-2**	**-45**	
7	**D to C**	**4**	**160-100**	**48-50**	**60**	**-2**	**-30**	**TRUE**
8	**C to B**	**4**	**200-160**	**46-48**	**40**	**-2**	**-20**	**TRUE**
9	**B to A**	**4**	**219-200**	**44-46**	**19**	**-2**	**-9.5**	**TRUE**
10	**A to MPP**	**4**	**220-219**	**42-44**	**1**	**-2**	**-0.5**	**TRUE**
11	**J to I**	**1**	**184-172**	**34-32**	**12**	**2**	**12-Feb**	
12	**I to H**	**1**	**195-184**	**36-34**	**11**	**2**	**11-Feb**	**11/2-12/2=-1/2**
13	**H to G**	**1**	**205-195**	**38-36**	**10**	**2**	**10-Feb**	**10/2-11/2=-1/2**
14	**G to F**	**1**	**215-205**	**40-38**	**10**	**2**	**10-Feb**	**10/2-10/2=0**
15	**F to MPP**	**1**	**220-215**	**42-40**	**5**	**2**	**05-Feb**	**5/2-10/2=-5/2**
16	**MPP to F**	**2**	**215-220**	**40-42**	**-5**	**-2**	**05-Feb**	
17	**F to G**	**2**	**205-215**	**38-40**	**-10**	**-2**	**10-Feb**	**10/2-5/2=5/2**
18	**G to H**	**2**	**195-205**	**36-38**	**-10**	**-2**	**10-Feb**	**10/2-10/2=0**
19	**H to I**	**2**	**184-195**	**34-36**	**-11**	**-2**	**11-Feb**	**11/2-10/2=1/2**
20	**I to J**	**2**	**172-184**	**32-34**	**-12**	**-2**	**12-Feb**	**12/2-11/2=1/2**

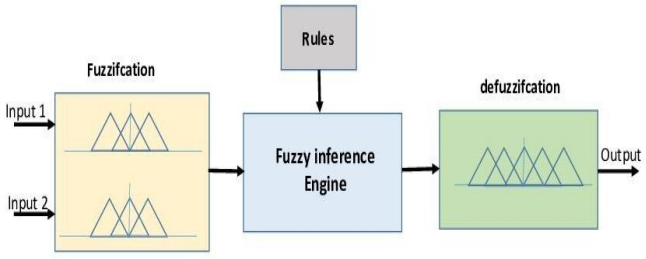

Figure 6. Diagrammatic representation of the suggested fuzzy logic system

V. DC-DC CONVERTERS PLAN AND USAGE

Having an electrical alteration, this convertor changes a deserted contribution DC vitality into a controlled one to urge a expected yield voltage. It includes electrical equipment that experiences a little power loss when linked to another device or when the input voltage is reduced. Figure 8 shows the visit chart for a boost-converter circuit. The values uncovered within the circuit were connected within the MATLAB program.

These are assigned for the purpose of explanation, promotion and sketch numerous signals denied of any connected intimation[22-24].

A. Operation of Step-up Converter

The measures of the circuit mechanisms (Figure 8) are assigned on each constituent. With a beat width achieving (PWM) event at 1000 Hz, the MOSFET acts in this circuit as an electric switch that shuts and opens at various periods..

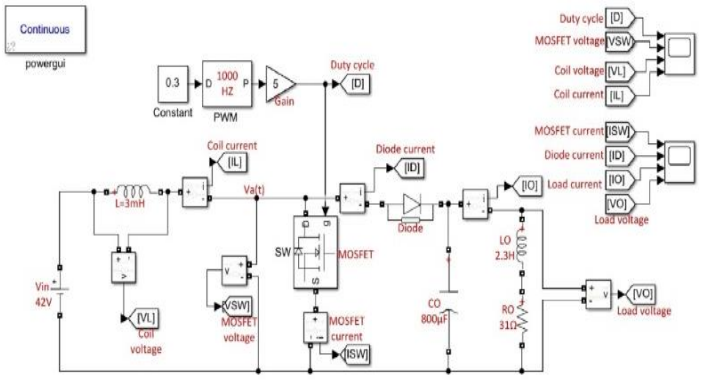

Figure 7. Boost converter circuit

The difference in the duty cycle wave (D) is shown in Figure 9(a), where T = Ton + The MOSFET closes at time Toff and opens at time Toff and Ton, which correspond to 0.3 and 0.7 of time T, respectively. When the MOSFET is turned on, there occurs an electronic transition (Diagram 9(b) It shorts out and creates zero voltage across its cross section (Va(t) = 0 V). For a retro of 0.3 T, the inductance is directly connected to the basis (Vin = 42 V). Fig. 9(c). The inductance's current is dependent on the period constant (= L / R) and does not fluctuate momentarily. The current continues to increase through the inductor for 0.3 T (Figure 9(d)), at which point its value is identical to the MOSFET current (Figure 910(a)). As a result, the coil's industrialized magnetic field contained vigor related to inductor production and current modification [25]. Since the voltage Va(t) = 0, the diode is oppositely biased (open circuit) in this instance. Due to the second stage's open circuit MOSFET (Toff = 0.7 T) and 0 duty cycle. The junction rectifier is momentarily biased forward (locked circuit), in series with the diode, and the spiral expands. The coil at this time Fig. 9(c). This circuit functions as a step-up converter when the productivity voltage is equal to the quantity of the input and inductor voltages. The capacitive load (CO) is sensitive throughout the MOSFET's open circuit. When the diode is in open circuit, the capacitance is cleared by the weight of the diode, and the value of the production current leftovers continues to depend on the capacitance value (Figure 910(c)). When the inductance is individually powered and cleaned of its vigor, the capacitive voltage is decreased and increased (Figure 910(c)) [26]. The inductance and capacitance limits in a post convertor are discovered via subsequent deals.

$$V_O = \frac{1}{1-D} V_{in} \quad (8)$$

$$I_{in} = \frac{1}{1-D} I_O \quad (9)$$

$$T = T_{on} + T_{off} \quad (10)$$

$$D = \frac{T_{on}}{T} \quad (11)$$

$$L = \frac{V_{in} \times D}{fs \times \Delta IL} = \frac{V_{in} \times (1-D) \times D}{fs \times \Delta IL} = \frac{R_O \times (1-D) \times D}{fs \times (\frac{\Delta IL}{I_O})} = \frac{V_{in} \times (V_O - V_{in})}{fs \times \Delta IL \times V_O} \quad (12)$$

$$\Delta IL = \frac{V_{in(min)} \times D}{fs \times L} = I_{in(max.)} - I_{in(min.)} = I_{L(max.)} - I_{L(min.)} \text{ Figure 8d} \quad (13)$$

For determining the inductor ripple (ΔIL) value, the output current was set between 0.2 and 0.4.[27].

$$\Delta IL = (0.2 \text{ to } 0.4) \times I_{O(max.)} \times \frac{V_O}{V_{in}} \quad (14)$$

$$C_{O(min.)} = \frac{I_{O(max.)} \times D}{fs \times \Delta V_O} \quad (15)$$

where V_O = output voltage, D = duty cycle, V_{in}= input voltage, L = inductor, I_{in} = input current, ΔIL = estimated inductor ripple current , I_O = output current, fs = switching frequency, R_O = load resistance, $V_{in(min)}$ = minimum input voltage, $I_{in(max.)}$ = maximum input current, $I_{in(min.)}$ = minimum input voltage, $I_{L(max.)}$ = maximum inductor current, $I_{L(min.)}$ = minimum inductor current, $C_{O(min.)}$ = minimum output capacitor, and ΔV_O = desired output ripple voltage

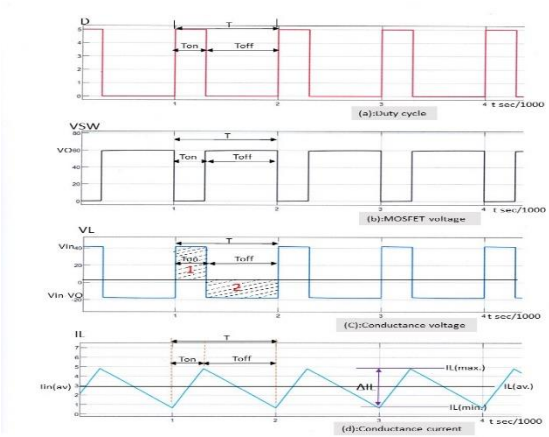

Figure 8. Difference in the (a) routine duties, (b) voltage on MOSFETs, (c) voltage on a conductor, and (d) current in a conductor

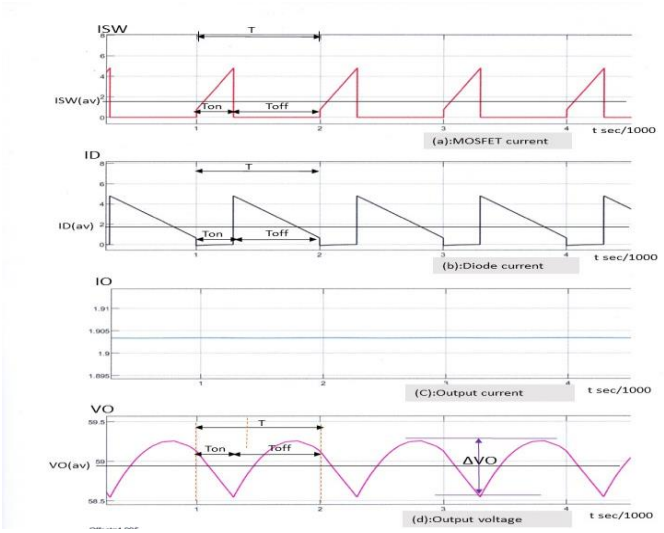

Figure 9. Variation in the (a) MOSFET i, (b) diode i, (c) output i, and (d) output v

B. Boost Converter Featuring an FLC and PV Array

Afterward replacement the DC foundation with a PV collection (as stated in), keeping the tour mechanisms the same but switching to PWM at a frequency of 3800 Hz, and replacing the duty-cycle (constant) with the FLC in Figure 8, the new circuit (Figure 11) was designed. The calculations from Figures 8 to 15 were rummaged-sale for further calculations. Through a post convertor and FLC, the PV array's MPP was skilfully applied to the occupied circuit.. The FLC circuit's internal details are shown in Figure 12. In! ., the association among the PV array's power and voltage was insufficient to allow the MPP to operate at a secure level of continuous solar irradiation and fever. The sun's energy value varied often during the day, boosting from low (in the morning) to high (with a peak at midday) before descending to actually low (at sunset). Figure 15, Figure 13 illustrates the relationship between the PV cell's current and power, showing how different geometries were distorted at various solar irradiances (300, 500, 800, and 1000 W/), utilizing the MATLAB code described in Figure 4. Different from how the sun irradiance affected things, The temperature remained steady and disrespected its impact on the PV cell's ability to perform differently. The PV cell was chosen and kept at a constant temperature of 25 °C during the testing in order to avoid the issues. Each sun irradiance level had four strongminded MPP norms. Additionally, it was anticipated that until

the point touched by A1 wherever the sun irradiance stabilised at 300 W/ till MPP1, both the power and the current would continue to be zero. All four forms were divided into two separate pieces, the first of which was placed on the MPP's right side and the second on its left. combined current

$$\Delta P = P(t) - P(t-1)$$

$$\Delta I = I(t) - I(t-1) \quad (16)$$

$$E(t) = \frac{\Delta P}{\Delta I} = \frac{P(t)-P(t-1)}{I(t)-I(t-1)} \quad (17)$$

$$CE(t) = E(t) - E(t-1)$$

wherever ΔI denotes the current's shifts, I(t) and I(t-1) denotes the currents at period t and (t-1), correspondingly, Additional cyphers have their normal sense.

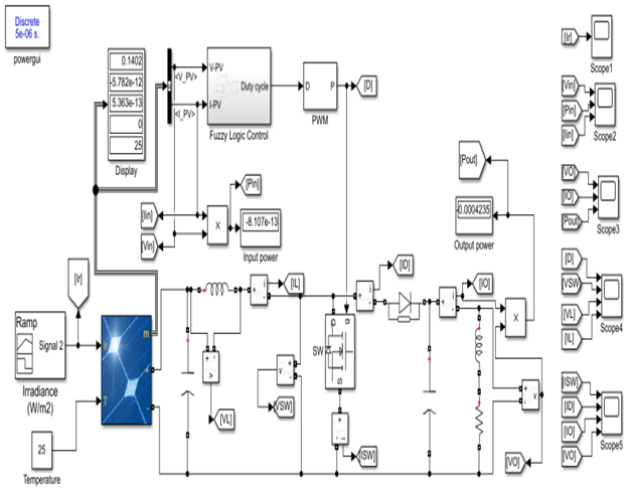

Figure 10.Project of the MPP tour by means of FLC procedure

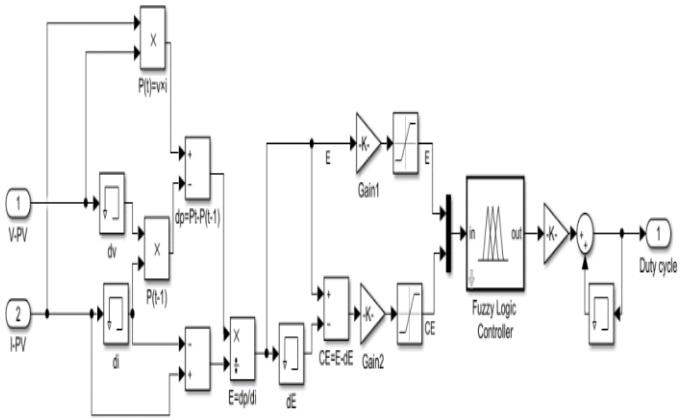

Figure 11. Circuit diagram of the FLC algorithm

The error was to consistently be pessimistic to negative to the right and to the left of the MPP. The amount of coldness of the point from the MPP was indicated by the error value after adding. Although the signal from the MPP indicated the way of drive in either the way of the MPP or in a retrogressive manner depending on the type of convertor employed, the alteration of error might also be negative or positive. The value indicated how quickly the point was being driven. The FLC compared the incorrect value and alteration of mistake conforming to those 49 fuzzy rules starting from point A1. The PV cell's power and current were identified as

Table 3. Explanation of the fuzzy rules

CE / E	NB	NM	NS	ZE	PS	PM	PB
NB	1 ZE	2 ZE	3 ZE	4 NB	5 NB	6 NB	7 NB
NM	8 ZE	9 ZE	10 ZE	11 NM	12 NM	13 NM	14 NM
NS	15 ZE	16 ZE	17 ZE	18 NS	19 NS	20 NS	21 NS
ZE	22 NS	23 NS	24 ZE	25 ZE	26 ZE	27 PS	28 PS
PS	29 PS	30 PS	31 PS	32 PS	33 ZE	34 ZE	35 ZE
PM	36 PM	37 PM	38 PM	39 PM	40 ZE	41 ZE	42 ZE
PB	43 PB	44 PB	45 PB	46 PB	47 ZE	48 ZE	49 ZE

enlists the duty-cycle (D) language values at which the PV collection's current or voltage was increased or decreased. When E was NS and CE was PB, for example, the duty cycle was NS. This suggested that it was intended to restore the point to the MPP by slightly lowering the value of D when the error was small and negative (i.e., to the right of the MPP and close to it) and when the error changed significantly and negatively (i.e., it strongly enthused against the MPP). In order to limit the rate at which D concluded its relationship with current and voltage, Eqs. 8 and 9 were employed (as well as lowering the value of figure 13. Therefore, any quantity of D was unnecessary since it may move the point away from the MPP, but the previous amount was enough to spread the MPP. The positive change in error in Area 2 (to the right of the MPP) suggested that the point was pushed against the MPP's methodology. Accordingly, a certain amount of D was required depending on the magnitude of the error and its change. Also prepared were regions 3 and 4. It was difficult to tell whether the point was to the right or left of the MPP since rules 22, 23, and 28 all had zero error, which made them interchangeable. Lastly, the (figure 13) Once the sun radiation changed, it somewhat enthused arbitrarily to the left or right of the MPP. The PV array was pompous by the difference of various concerns such as infection, sun radiation, load current (alteration in resistance), and others because of its non-linear landscape.

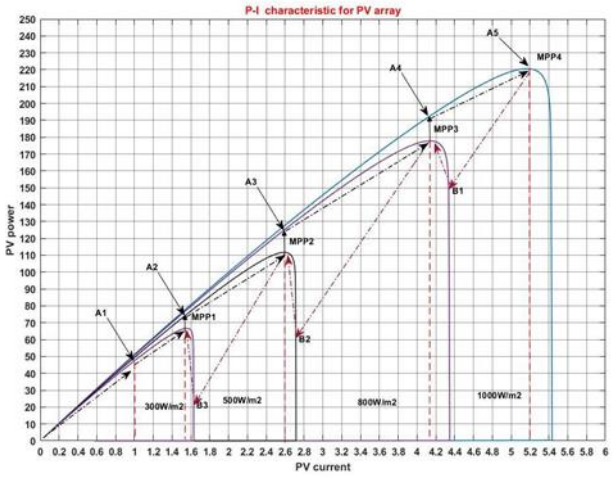

Figure 12. Features of the PV array's power and voltage

A respectable outcome. It was delta D (D) for the output; thus, a narrow output border was used to ensure that the step amount didn't get too small. The duty-cycle value was divided into 100 parts as a result of a very small variation (between zero and one). For instance, depending on where the point from the MPP was located, a fraction of 100 was added or subtracted to the previous number each time. If the D was alienated into a tiny quantity, the MPP achievement the procedure was protracted. The consistency was also lost for a significant amount of separation and swung around the MPP, making the scheme imbalanced. Therefore, it was desired to improve the production in order to maintain the value.a respectable outcome. It was delta D (D) for the output; thus, a narrow output border was used to ensure that the step amount didn't get too small. The duty-cycle value was divided into 100 parts as a result of a very small variation (between zero and one). For instance, depending on where the point from the MPP was located, a fraction of 100 was added or subtracted to the previous number each time. If the D

was alienated into a tiny quantity, the MPP achievement the procedure was protracted. The consistency was also lost for a significant amount of separation and swung around the MPP, making the scheme imbalanced. Therefore, it was desired to improve the production in order to maintain the value**.**

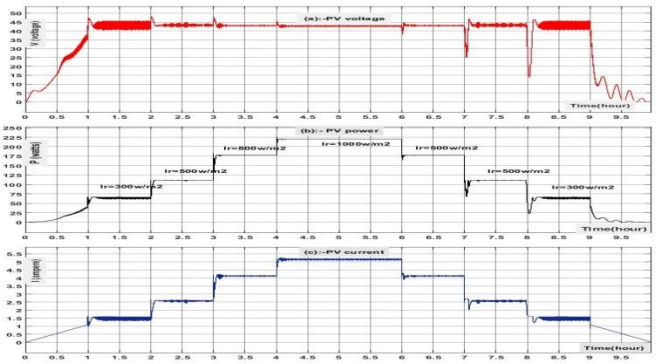

Prior to attaching the FLC, measuring the input signal, the association function's boundaries were carefully set. Then, a modification was applied to raise or lower the standards for further regulation, procuring a a respectable outcome. It was delta D (D) for the output; thus, a narrow output border was used to ensure that the step amount didn't get too small. The duty-cycle value was divided into 100 parts as a result of a very small variation (between zero and one). For instance, depending on where the point from the MPP was located, a fraction of 100 was added or subtracted to the previous number each time. If the D was alienated into a tiny quantity, the MPP achievement the procedure was protracted. The consistency was also lost for a significant amount of separation and swung around the MPP, making the scheme imbalanced. Therefore, it was desired to improve the production in order to maintain the value.

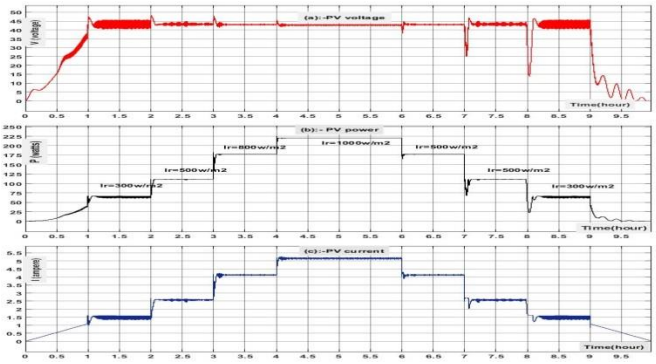

Figure 13. Association functions for the adjustable (a) input (E), (b) input (CE), and (c) output (D).

Figure 16 illustrates that the PV cell power was at the highest possible level of each quantity of solar radiation throughout the MATLAB research, and Figure 17 displays that the output power was at the highest level, and the output voltage was amplified because we used a step-up converter (boost converter).

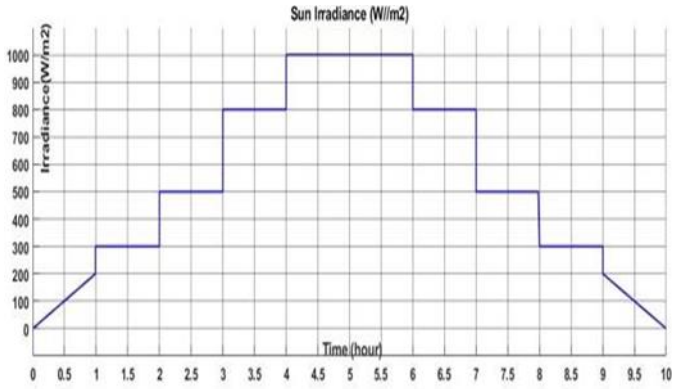

Figure 14. Solar irradiance scheme

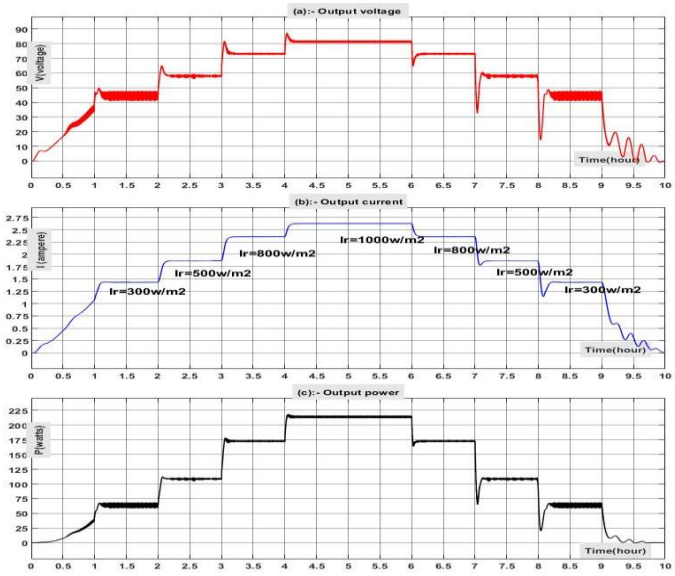

Figure 15. PV collection (a) voltage, (b) power, and (c) current

C. Operation of Step-down Converter

A step-down (buck converter) is shown in Figure 18 where the PV collection was not employed as the circuit's foundation and the boost converter's output was the voltage source (Figure 11). With the exception of the PWM, the circuit's other components were identical to those in the previous one. (functioned at the frequency of 5300 Hz). The diode turned off when the MOSFET turned on (at period t = 0.6T), indicating that it was 60% on and 40% off over the full-time intermission of T.

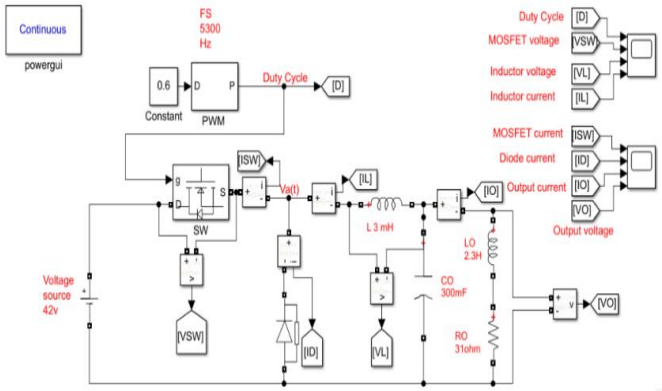

Figure 16. Buck converter circuit diagram

Figure 19(a) shows that the inductor's current did not alteration suddenly but rather was dependent on the period constant (= L / R). Due to a short circuit, the MOSFET had zero voltage running through it (Figure 19(b)). The diode's voltage was the basis voltage and became Va(t) = Vin since the circuit was open, but the voltage crossways the inductor was (Vin - Vout) (Figure 19(c)). In reality, the MOSFET developed off when the inductor current gradually increased (Figure 19(d)). At this point, the inductor stored energy as an attractive field that was dependent on the inductor's value (L) and current variation. In the second stage, the inductor returned the stowed energy when the MOSFET was off and the diode was on[28, 29].

$$D = \frac{V_O}{V_{in}} \tag{18}$$

$$L = \frac{V_O \times (1-D)}{fs \times \Delta IL} = \frac{I_O \times R_O \times (1-D)}{fs \times \Delta IL} = \frac{R_O \times (1-D)}{fs \times (\frac{\Delta IL}{I_O})} = \frac{V_O \times (V_{in} - V_O)}{fs \times \Delta IL \times V_{in}} \tag{19}$$

$$\Delta IL = \frac{(V_{in(max.)} - V_O) \times D}{fs \times L} = I_{L(max.)} - I_{L(min.)} \tag{20}$$

To estimate the value of an inductor ripple ΔIL, it is selected between (0.2 to 0.4) of the output current

$$\Delta IL = (0.2 \text{ to } 0.4) \times I_{O(max.)} \quad (21)$$

$$C_{O(min.)} = \frac{\Delta IL}{8 \times fs \times \Delta V_O} \quad (22)$$

where V_O = output voltage, D = duty cycle, V_{in} = input voltage, L = inductor, I_{in} = input current, ΔIL = estimated inductor ripple current, I_O = output current, fs = switching frequency, R_O = load resistance, $V_{in(min)}$ = minimum input voltage, $I_{in(max.)}$ = maximum input current, $I_{in(min.)}$ = minimum input voltage, $I_{L(max.)}$ = maximum inductor current, $I_{L(min.)}$ = minimum inductor current, $C_{O(min.)}$ = minimum output capacitor, ΔV_O = desired output ripple voltage [18].

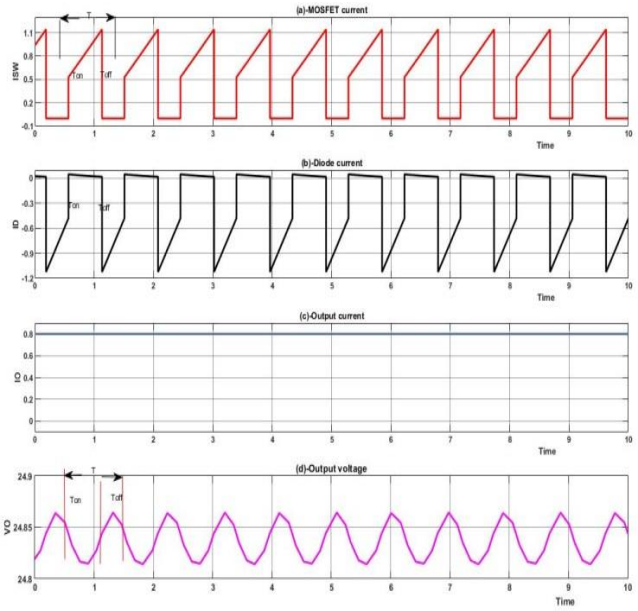

Figure 17. (a) MOSFET current, (b) current via a diode, (c) current coming out, and (d) voltage at output

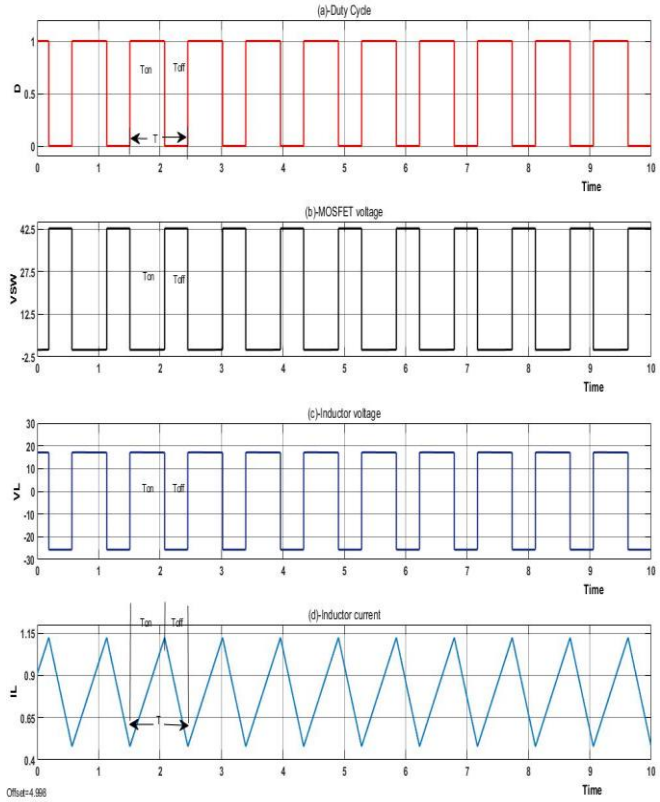

Figure 19. (a) Duty sequence, (b) MOSFET voltage, (c) inductance voltage, and (d) inductance current

VI. PROPOSED CIRCUIT MPP AND AVR COMBINATION

The final circuit, which generated the greatest power from the PV array and steady voltage for the generator's excitation field coil, was built by connecting this AVR as exposed in Figure 21. The PWM frequencies and the values of the circuit components were left unchanged. Figure 16's solar radiation was changed from a low to a high value before being dropped (to replicate a genuine circumstance), and Figure 22(c) shows the maximum power of the PV array at each value. Figure 22(a) and (b) illustrate the voltage and current of the PV array, respectively. Figure 22(c) shows the reference voltage and synchronous generator voltage at which the FLC might function in the field.

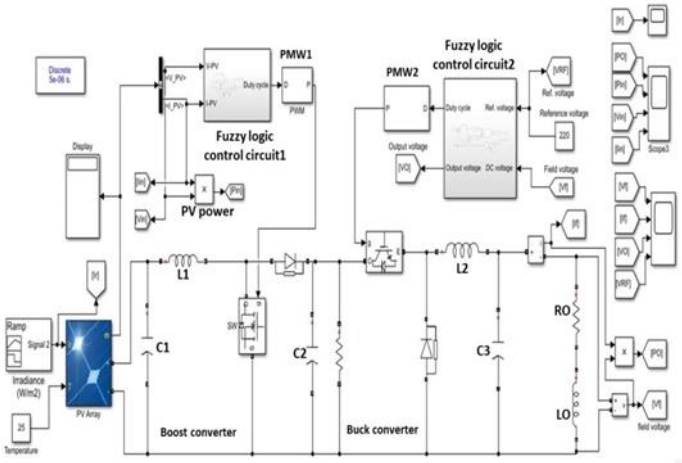

Figure 20. Final circuit boost and buck converters with AVR Combination

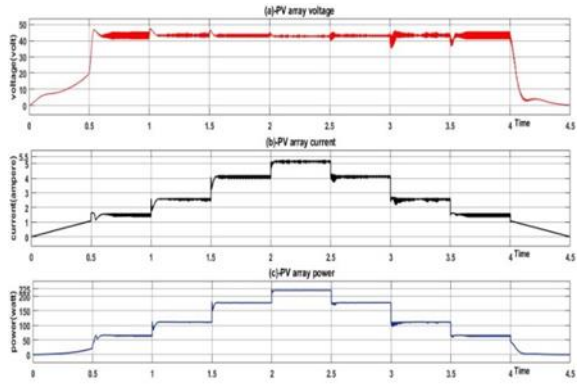

Figure 21. PV array (a) voltage, (b) current, and (c) power

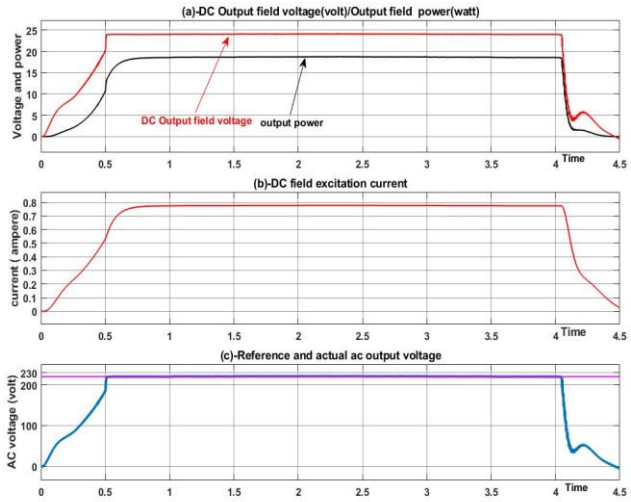

Figure 22. (a) DC voltage and power output from buck converters for field excitation coils, (b) DC field amplification current and (c) real and reference ac output voltage.

VII. SIMULATION OUTCOMES

The solar radiation was separated into nine portions, each of which represented a distinct unit of time at constant temperature. Furthermore, it was assumed that the typical duration of sunlight would be nine hours, with each part of the time unit denoting an hour. The sun radiation was equally distributed on each side of the 1000 W/all-out figure. The circuit was verified for 300, 500, and 800 W/in addition to the ludicrous worth of 1000 W/and then compared to the characteristics indicated in MATLAB for the specified constraints of the PV exhibit. The consequences exposed that the correctness was actual high with a regular of 98.875.

VIII. CONCLUSION

This paper reports the realization of a novel artificial intelligence fuzzy controller with solar irradiance-altered maximum power. The proposed system achieved MPP in the first stage wherein it ensured the maintenance of the output voltage of the synchronous generator in the second stage. Four different states of the solar radiation were studied with an observation of the system's response to those states. The Simulink /MATLAB programs were developed to perform the experiment. The generator's excitation field voltage was controlled via a PD-like fuzzy control circuit, operating as an AVR back-feeding. The feedback from the 220 V generator output was compared with the reference voltage and errors. The accuracy of the system in the first stage of the MPP algorithm was in the range of 96.7 to 99.8 %. On top, the stability of the voltage and current of the excitation field was very high. Even at low solar irradiance (300 W/m^2), the power or voltage phase of the combined system (MPP and AVR) revealed high stability. The output voltage did not change despite a sudden change in the solar irradiance. In short, the proposed system can be practically adopted with high reliability due to the low-cost materials' components use and ease of design.

ACKNOWLEDGMENT

Abdullah is thankful to Dr.S.K.Ghushal for many valuable suggestions and critical readings of the manuscript

REFERENCES

[1] Wu, T., et al., The main progress of perovskite solar cells in 2020–2021. Nano-Micro Letters, 2021. 13: p. 1-18.

[2] Ehrlich, R. and H.A. Geller, Renewable energy: a first course. 2017: CRC press.

[3] Xu, L., R. Cheng, and J. Yang, A new MPPT technique for fast and efficient tracking under fast varying solar irradiation and load resistance. International Journal of Photoenergy, 2020. 2020: p. 1-18.

[4] Kumar, D. and R. Raushan. PV Array Dynamic Reconfiguration by leveling the Solar Irradiance under Partial Shading Conditions. in 2022 2nd International Conference on Emerging Frontiers in Electrical and Electronic Technologies (ICEFEET). 2022.

[5] Mahdi, A.S., et al., Maximum power point tracking using perturb and observe, fuzzy logic and ANFIS. SN Applied Sciences, 2019. 2(1): p. 89.

[6] Bouarroudj, N., et al., Fuzzy logic controller based maximum power point tracking and its optimal tuning in photovoltaic systems. Serbian Journal of Electrical Engineering, 2021. 18: p. 351-384.

[7] Raj, M.P. and A.M. Joshua. Design, implementation and performance analysis of a LabVIEW based fuzzy logic MPPT controller for stand-alone PV systems. in 2017 IEEE International Conference on Power, Control, Signals and Instrumentation Engineering (ICPCSI). 2017. IEEE.

[8] Mustafić, D., et al. Implementation of Incremental Conductance MPPT Algorithm in Real Time in Matlab/Simulink Environment with Humusoft MF634 Board. in 2020 9th Mediterranean Conference on Embedded Computing (MECO). 2020. IEEE.

[9] Guettaf, S.E.I., et al. A modified maximum power point tracking controller based on the perturb and observe algorithm used for solar energy system. in Artificial Intelligence and Renewables Towards an Energy Transition 4. 2021. Springer.

[10] Belhimer, S., M. Haddadi, and A. Mellit, A novel hybrid boost converter with extended duty cycles range for tracking the maximum power point in photovoltaic system applications. International journal of hydrogen energy, 2018. 43(14): p. 6887-6898.

[11] Qiao, W. and Q. Hui. Energy-based hybrid excitation control for synchronous generators. in IEEE PES General Meeting. 2010. IEEE.

[12] Kim, J.-C., J.-H. Huh, and J.-S. Ko, Optimization design and test bed of fuzzy control rule base for PV system MPPT in micro grid. Sustainability, 2020. 12(9): p. 3763.

[13] Chen, Y.-T., Y.-C. Jhang, and R.-H. Liang, A fuzzy-logic based auto-scaling variable step-size MPPT method for PV systems. Solar Energy, 2016. 126: p. 53-63.

[14] Prasad, C.B., et al. A fuzzy logic based MPPT method for solar power generation. in 2017 International Conference on Intelligent Computing and Control Systems (ICICCS). 2017. IEEE.

[15] Siddula, S. Analysis of fuzzy logic based MPPT using Incremental Conductance technique for PV cell. in 2020 International Conference on Smart Technologies in Computing, Electrical and Electronics (ICSTCEE). 2020. IEEE.

[16] Sarvi, M. and A. Azadian, A comprehensive review and classified comparison of MPPT algorithms in PV systems. Energy Systems, 2022. 13(2): p. 281-320.

[17] Verma, P., R. Garg, and P. Mahajan, Asymmetrical interval type-2 fuzzy logic control based MPPT tuning for PV system under partial shading condition. ISA transactions, 2020. 100: p. 251-263.

[18] Shyni, S. and R. Ramadevi, Design of fuzzy logic controller for fused Luo converter based solar/wind hybrid green energy system. Environment, Development and Sustainability, 2021: p. 1-24.

[19] Shufian, A., et al. Modeling & Economical Analysis of Hybrid Solar-Wind-Biomass-H 2-based Optimal Islanding Microgrid in Bangladesh. in 2022 IEEE 10th Region 10 Humanitarian Technology Conference (R10-HTC). 2022. IEEE.

[20] Zhang, W. and A. Maleki, Modeling and optimization of a stand-alone desalination plant powered by solar/wind energies based on back-up systems using a hybrid algorithm. Energy, 2022. 254: p. 124341.

[21] Bhukya, L. and S. Nandiraju, A novel photovoltaic maximum power point tracking technique based on grasshopper optimized fuzzy logic approach. International Journal of Hydrogen Energy, 2020. 45(16): p. 9416-9427.

[22] Li, X., et al., A novel beta parameter based fuzzy-logic controller for photovoltaic MPPT application. Renewable energy, 2019. 130: p. 416-427.

[23] Subramanian, V., et al., Modeling and analysis of PV system with fuzzy logic MPPT technique for a DC microgrid under variable atmospheric conditions. Electronics, 2021. 10(20): p. 2541.

[24] Ali, M.N., et al., Promising MPPT methods combining metaheuristic, fuzzy-logic and ANN techniques for grid-connected photovoltaic. Sensors, 2021. 21(4): p. 1244.

[25] Rashid, M.H., Power electronics handbook. 2017: Butterworth-heinemann.

[26] Skvarenina, T.L., The power electronics handbook. 2018: CRC press.

[27] Hagedorn, J., Basic calculations of a 4 switch buck-boost power stage. SLVA535B. Texas Instruments, Dallas, Texas, USA, Rep, 2018.

[28] Cobos, J.A., et al. Differential power as a metric to optimize power converters and architectures. in 2017 IEEE Energy Conversion Congress and Exposition (ECCE). 2017. IEEE.

[29] Halder, T. An Impact of the Voltage & Current Ripples in the Power Stages of the Boost Converter. in 2018 IEEE Electron Devices Kolkata Conference (EDKCON). 2018. IEEE.